JOURNAL OF SOLID STATE CHEMISTRY 112, 182–188 (1994)

Powder Diffraction Studies in the $YONO_3$–Y_2O_3 System

D. Pelloquin,[1] M. Louër, and D. Louër

Laboratoire de Cristallochimie (URA CNRS 1495), Université de Rennes, Avenue du Général Leclerc, 35042 Rennes cedex, France

Received June 9, 1993; accepted October 6, 1993

The crystal structure of yttrium oxide nitrate and the microstructure of the oxide obtained from its thermal decomposition have been investigated by modern powder diffraction methods. Sequential high-temperature diffraction studies of the thermal decomposition of two precursors of yttrium oxide nitrate, i.e., neutral yttrium nitrate and yttrium hydroxide nitrate, are reported. The structure of $YONO_3$ has been determined *ab initio* from conventional powder diffractometry using monochromatic X-rays. The pattern was indexed by the successive dichotomy method yielding tetragonal unit cell dimensions: $a = 3.8590(1)$ Å and $c = 9.7161(6)$ Å. The space group is $P4/nmm$ and $Z = 2$. Most of the atoms were located by direct methods and the remaining ones from a Fourier map. Refinement of the complete diffraction profile parameters converged to final agreement factors $R_p = 0.12$, $R_{wp} = 0.16$ and $R_F = 0.039$. The structure is closely related to the matlockite PbFCl-type structure. The microstructure of ex-oxide–nitrate yttrium oxide has been analysed by total pattern fitting techniques, from which strain-free coherently diffracting nanodomains with a rectangular parallelepipedic shape have been obtained.

INTRODUCTION

Yttrium oxide nitrate is formed during the thermal decomposition of yttrium nitrate pentahydrate (1). It is air sensitive and obtained in powder form after the successive decomposition of intermediate hydrates. Compared to the chemically related oxide halides which show a well-known PbFCl (matlockite) type structure (see, for example, Ref. (2)), no structural data have been reported for $YONO_3$. Moreover, as a consequence of the low thermal stability of the nitrate groups, the decomposition of nitrate precursors leads to oxides with fine particles. Previous studies have demonstrated that the microstructural features (crystallite sizes and morphology, microstrains, stacking faults) of the nanoscale particles formed are dependent on the precursor (3, 4) and that they are qualitatively not modified during the initial stages of crystallite growth (5, 6). The purpose of the present study was to investigate the structure of yttrium oxide nitrate and the characteristics of the microstructure of its decomposition product Y_2O_3. In order to obtain a material with good crystallinity, the thermal behaviour of yttrium nitrate pentahydrate has been studied by sequential thermodiffractometric analysis. Another route for obtaining $YONO_3$ from yttrium hydroxide nitrate, a binder described by Holcombe (7), has also been investigated. This investigation deals with the characterization, by means of modern powder diffraction techniques, of the thermal decomposition of the two precursors, the structure determination of yttrium oxide nitrate and the microstructure of the corresponding yttrium oxide.

EXPERIMENTAL CONSIDERATIONS

Materials

The compound $Y(NO_3)_3 \cdot 5H_2O$ was supplied by Aldrich (No. 23, 795-7). The nonstoichiometric yttrium hydroxide nitrate described by Holcombe (7) was prepared by an interdiffusion method in aqueous solutions (8). Using a pipette, a 2 *M* solution of yttrium nitrate was introduced into a glass container which was three-quarter full of distilled water. The container was connected to a similar one filled with 2 *M* ammonia. After three days, a powder of yttrium hydroxide nitrate is obtained. It has been identified by its powder diffraction pattern, the TG measurements were consistent with the formula $Y_2(OH)_{5.1}(NO_3)_{0.9} \cdot H_2O$ previously reported (7).

Sequential Thermodiffractometric Analysis

For the high-temperature X-ray diffraction experiments (HTXRD), powder diffraction data were collected with a INEL (CPS 120) curved position sensitive detector, which allows simultaneous data recording of a diffraction pattern over a range of 120°. The detector was used in a semifocusing geometry by reflection, described elsewhere (9). Strictly monochromatic Cu$K\alpha_1$ radiation ($\lambda = 1.54059$ Å) was selected using an incident-beam curved-quartz monochromator with asymmetric focusing (short focal distance = 130 mm, long focal distance = 510 mm). The

[1] Present address: Laboratoire CRISMAT, ISMRA, 6 Bd du Maréchal Juin, 14050 Caen cedex, France.

0022-4596/94 $6.00

stationary powder sample is located at the center of the goniometer (R = 250 mm) and intercepts the convergent X-ray beam, which is focused on the goniometer circle. A fixed θ_i angle of 6° between the incident beam and the surface of the sample was selected. Data acquisition was performed by the PSD with a spatial resolution of about 0.03° (2θ). Samples were located in a monitored high-temperature device (Rigaku). Experiments were carried out under nitrogen gas with a heating rate of 10°C · hr^{-1}. To ensure satisfactory counting statistics an interval time of 2150 sec between two successive powder diffraction patterns was selected, including a counting time of 2000 sec.

High-Resolution Powder Diffractometry

For precise powder diffraction data a D500 Siemens powder diffraction system with a Bragg-Brentano geometry was used. Pure Cu$K\alpha_1$ radiation was produced with an incident beam curved-crystal germanium monochromator with asymmetric focusing (short focal distance = 124 mm, long focal distance = 216 mm). The adjustment of the diffractometer was checked by using standard reference materials. The instrumental resolution function (IRF) of this conventional powder diffractometer has a minimum of 0.065°(2θ) and shows twice this value at 130°(2θ) (10). The sample was located in a tight sample holder designed for preserving a specimen under nitrogen gas. The powder diffraction pattern of yttrium oxide nitrate was scanned in steps of 0.02°(2θ) and a fixed counting time (12 sec) was employed. For the structure analysis the stability of the incident beam was checked by measuring again the first few lines of the pattern. A precise determination of peak positions and integrated intensities was carried out by means of the fitting program FIT available in the PC software package DIFFRAC-AT, supplied by Siemens/Socabim. A preliminary pattern decomposition analysis revealed anisotropic diffraction line broadening, but from the scatter of peak's full widths at half maximum (FWHM) it was not possible to describe their angular dependence as a function of the direction of diffraction vectors, though it would have been desirable in subsequent Rietveld refinements (11).

THERMAL ANALYSIS OF PRECURSORS AND MICROSTRUCTURE OF YTTRIUM OXIDE

Figure 1 shows a three-dimensional representation of the successive powder diffraction patterns during the decomposition of yttrium nitrate pentahydrate in the range 20–500°C. It shows that the decomposition of the precursor into yttrium oxide occurs in five successive steps. All phases have been identified from the work of Odent and Autrusseau-Duperray (1), i.e. the hydrates with 3 and 1 water molecules, the anhydrous phase, the oxide nitrate and finally Y_2O_3. The pattern of yttrium oxide nitrate is characterized by broad diffraction lines owing to the successive thermal decomposition of the hydrated phases. The crystal structure of the hydrates with five, three and one water molecules were known (12–14), whereas the structure of the anhydrous and oxide nitrate phases remained unknown. Fig. 2 shows the 3D plot of the diffraction patterns during the thermal decomposition of yttrium hydroxide nitrate. Between 50 and 220°C two phases, not identified, are observed; then yttrium oxide nitrate is

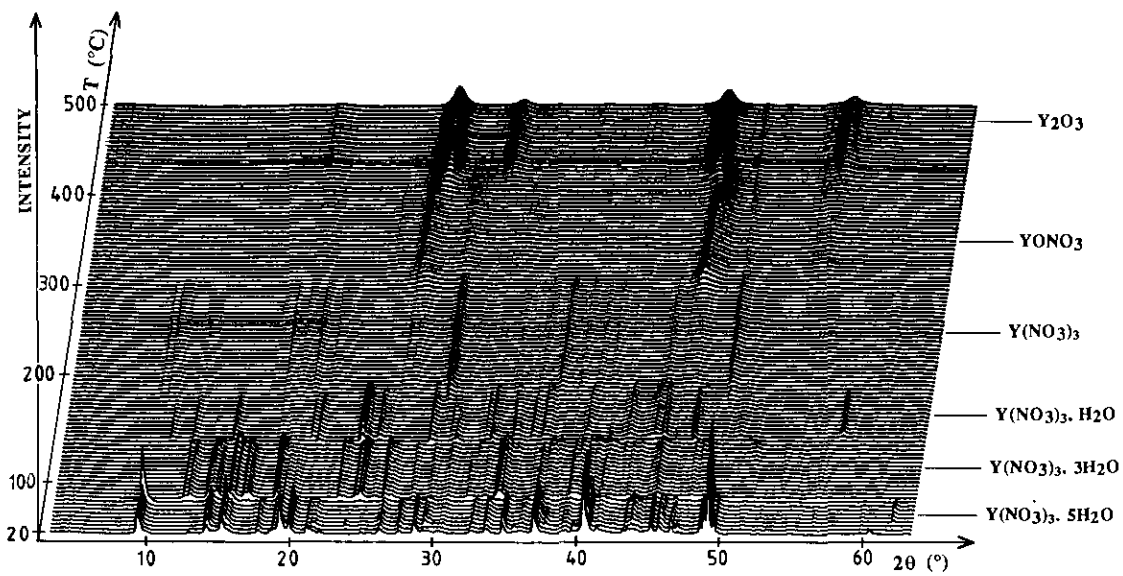

FIG. 1. HTXRD plot of $Y(NO_3)_3 \cdot 5H_2O$ in a nitrogen flow (heating rate: 10°C · hr^{-1}).

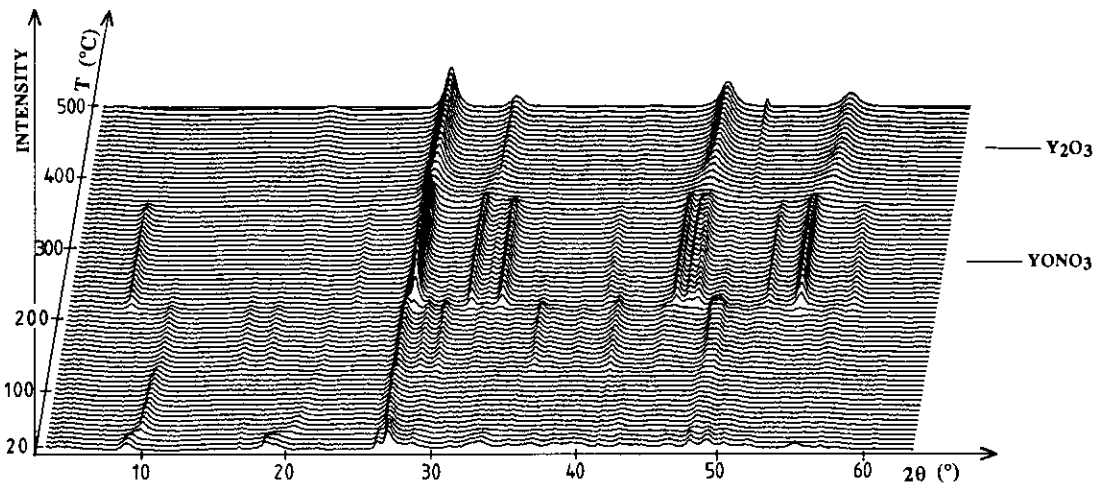

FIG. 2. HTXRD plot of $Y_2(OH)_{5.1}(NO_3)_{0.9} \cdot 5H_2O$ in nitrogen (heating rate: 10°C · hr^{-1}).

obtained before appearance of the oxide. We may notice that the oxide nitrate is formed at 220°C, i.e., 100° below the formation temperature from the former precursor. Comparison of the diffraction patterns of $YONO_3$ shown in Figs. 1 and 2 reveals a better crystallinity of the sample obtained from the later precursor. This sample was used in the subsequent structure analysis.

The microstructure of cubic yttrium oxide obtained from thermal decomposition of the neutral nitrate (heating rate 20°C · hr^{-1}) has been investigated by diffraction line broadening analysis after total pattern decomposition, from which the integral breadths β (area/peak intensity) of individual reflections were extracted. The complete procedure used in the analysis has recently been reported (4). Correction for instrumental contribution was based on the assumption that line profiles are Voigtian, which was in accordance with the observed Voigt parameter ϕ (=FWHM/β) lying between the Lorentzian (ϕ = 0.634) and the Gaussian (ϕ = 0.939) limits for all investigated lines. To correct the breadths of the observed reflections for instrumental broadening, the breadths of the instrumental lines were obtained from a sample of an annealed BaF_2 standard material desribed elsewhere (10). Two samples of ex-oxide-nitrate yttrium oxide, obtained at 800 and 950°C, were selected for the microstructural study; but for samples obtained at lower temperatures the diffraction lines were too broad for a precise analysis. The Williamson–Hall plot, in which β_f in reciprocal units ($=\beta_{f(2\theta)} \cos \theta/\lambda$) is plotted as a function of d* ($=2 \sin \theta/\lambda$) were obtained for the two samples. Figure 3 shows the plot for the sample prepared at 800°C. It is immediately apparent that there is little scatter of β_f values on the total angular range, which indicates that the material is strain-free, and that the average zero-slope line has a nonzero intercept owing to the relatively small size of the coherently diffracting domains. β_f values can thus be attributed exclusively to size effects and β_f^{-1} (ε_β) is the volume-weighted average thickness of crystallites in the direction of the diffraction vector. ε_β is an apparent size; in order to relate it to actual mean dimensions, it has been assumed that, in the average, the crystallites have the shape of a rectangular parallelepiped, for which equations have been recently been reported (15). A least-squares refinement procedure from the individual apparent sizes was used for modelling the morphology of the crystallites. The dimensions obtained were 304 × 335 × 860 Å, close to a tetragonal shape. A similar analysis carried out on a sample obtained at 950°C led to the dimensions 488 × 572 × 890 Å. Until now few strain-free oxides with nanoparticles obtained by thermal decomposition of a precursor have been reported (3, 4), so it is interesting to note that ex-oxide-nitrate yttrium oxide has also negligible microstrains and could be a candidate as a standard reference material with small size crystallites, which can be monitored by acting on the thermal conditions of their preparation.

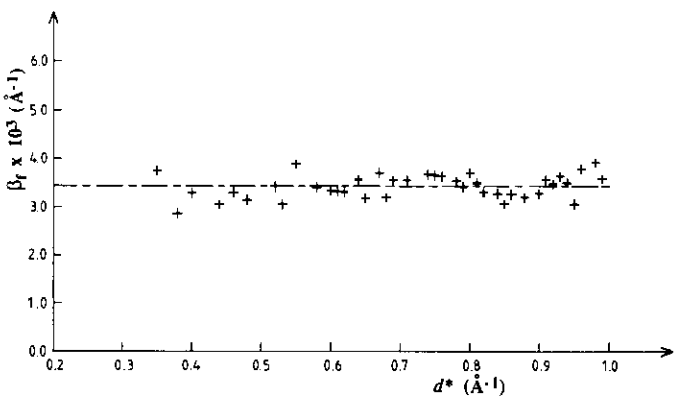

FIG. 3. Williamson–Hall plot of Y_2O_3 at 800°C (β_f versus d^*).

AB INITIO STRUCTURE DETERMINATION OF $YONO_3$

Indexing

Indexing of the powder diffraction pattern was performed by the successive dichotomy method (16), with the program DICVOL91 (17), which tackles any system, including triclinic. The first 20 lines were completely indexed on the basis of a tetragonal cell characterized by the figures of merit M_{20} = 131 and F_{20} = 125(0.0064, 25). This solution was used for reviewing the powder diffraction data available (43 lines) by means of the computer program NBS * AIDS83 (18). From this evaluation of data quality and refinement, the cell dimensions are found to be: a = 3.8590(1) Å and c = 9.7161(6) Å, V = 144.7 Å^3. From the pattern indexes with this unit cell, there is evidence for systematic absences consistent with the space groups $P4/nmm$ or $P4/n$. The final figures of merit, calculated with systematic absences not included in the number of theoretical lines, are M_{20} = 112 and F_{30} = 107(0.007, 37) and the list of observed and calculated peak positions is given in Table 1. Using the PDF database (19), it was found that a similar unit cell was suggested for $GdONO_3$ (20), for which the crystal structure has not been reported. Consequently the ab initio structure determination of yttrium oxide nitrate has been carried out, using the space group with higher symmetry.

Structure Solution and Refinement

Integrated intensities obtained in the range 7–100°(2θ) were extracted by an iterative procedure for whole pattern fitting implemented in the Rietveld refinement program FULLPROF (21) based on the program described by Wiles & Young (22). From the pattern matching option 63 values of F_{obs} were obtained and introduced in the structure determination software package MolEN supplied by Enraf Nonius and running on a microvax computer. Atomic coordinates of Y, N and one O atoms were detected by the direct methods (program MULTAN). One Fourier difference map revealed the positions of the two remaining O atoms belonging to the nitrate group. The initial positions of these five independent atoms suggested the following remarks:

(i) All atoms lie in special positions and the space group $P4/n$ would lead to a similar result.

(ii) The nitrogen atom and one of its oxygen atom are located in a $4mm$ site. This is not consistent with the triangular geometry of a nitrate group, unless we consider a disorder of the two other oxygen atoms leading to two statistical orientations of the nitrate group. This problem could be avoided assuming the orthorhombic $Pmmn$ or $Pmn2_1$ subgroups. So the structure was solved again in the orthorhombic symmetry (105 F_{obs}). The Fourier difference map exhibited also two orientations of the nitrate group.

TABLE 1

X-Ray Powder Diffraction Pattern of $YONO_3$

h k l	$2\theta_{obs}$ (°)	$2\theta_{calc}$ (°)	d_{obs} (Å)	I_{obs}
0 0 1	9.089	9.094	9.72	49
1 0 1	24.819	24.805	3.584	17
0 0 3	27.500	27.518	3.241	3
1 0 2	29.540	29.538	3.021	100
1 1 0	32.804	32.974	2.728	44
1 1 1	34.118	34.101	2.626	8
1 0 3	36.185	36.179	2.4804	19
0 0 4	36.978	36.978	2.4290	4
1 1 2	37.799	37.783	2.3781	2
1 1 3	43.326	43.324	2.0867	12
1 0 4	44.012	44.013	2.0557	2
2 0 0	47.066	47.590	1.9292	27
2 0 1	48.045	48.035	1.8922	11
1 1 4	50.263	50.246	1.8137	13
2 0 2	50.881	50.879	1.7932	3
1 0 5	52.707	52.696	1.7353	3
2 1 1	53.924	53.915	1.6989	13
2 0 3	55.393	55.382	1.6573	3
2 1 2	56.543	56.546	1.6263	24
1 1 5	58.235	58.241	1.5830	6
2 1 3	60.758	60.763	1.5232	6
2 0 4	61.308	61.307	1.5108	5
1 0 6	62.111	62.111	1.4932	3
2 2 0	68.742	68.747	1.3644	4
2 2 1	69.534	69.518	1.3508	3
2 2 2	71.819	71.808	1.3134	2
1 0 7	72.277	72.281	1.3062	2
2 1 5	73.288	73.305	1.2906	2
3 0 1	74.322	74.322	1.2752	2
2 2 3	75.559	75.561	1.2574	2
3 0 2	76.557	76.555	1.2435	5
3 1 0	78.270	78.281	1.2205	5
3 1 1	79.001	79.016	1.2110	3
3 0 3	80.241	80.232	1.1954	3
2 2 4	80.728	80.715	1.1894	4
2 1 6	81.435	81.431	1.1808	3
3 1 3	84.846	84.838	1.1419	2
3 1 4	89.871	89.887	1.0906	5
2 1 7	90.827	90.826	1.0816	3
3 2 1	92.761	92.782	1.0640	2
3 2 2	94.951	94.947	1.0452	4
3 1 5	96.378	96.382	1.0335	3
3 2 3	98.566	98.575	1.0163	2

Nevertheless, all possible orthorhombic and tetragonal space groups were successively tried, leading to similar final agreement factors (R_F = 0.04). But the $P4/nmm$ space group was considered as the most convenient to describe the structure of $YONO_3$ (see discussion below).

The approximate coordinates of the five independent atoms were used as a starting model in the Rietveld method and refined isotropically. A Pearson VII function was selected to describe individual line profiles, with a possible angular variation of the shape factor m. Integrated intensities were distributed over five FWHM on

TABLE 2

Details of the Rietveld Full-Profile-Refinement for $YONO_3$

Space group	*P4/nmm*
Z	2
Wavelength (Å)	1.540598
2θ range (°)	20-100
Step increment (°2θ)	0.02
No. of reflections	63
No. of structural parameters	12
No. of profile parameters	20
No. of atoms	5
R_F	0.039
R_B	0.054
R_p	0.126
R_{wp}	0.162

Note. The *R* factors are defined as

$$R_F = \frac{\Sigma|I(\text{obs})^{1/2} - I(\text{calc})^{1/2}|}{\Sigma I(\text{obs})^{1/2}},$$

$$R_B = \frac{\Sigma|I(\text{obs}) - I(\text{calc})|}{\Sigma I(\text{obs})},$$

$$R_{wp} = \left\{\frac{\Sigma w_i[y_i(\text{obs}) - (1/c)y_i(\text{calc})]^2}{\Sigma w_i[y_i(\text{obs})]^2}\right\}^{1/2},$$

$$R_p = \frac{\Sigma|y_i(\text{obs}) - (1/c)y_i(\text{calc})|}{\Sigma y_i(\text{obs})}.$$

either side of a diffraction line. In order to describe the angular dependence of peak half-width, the usual quadratic form in tan θ was used and the initial values of the constants *U*, *V*, and *W* were derived from the fitting of some individual lines. Unit-cell and instrument parameters were allowed to vary from time to time during the refinement process. A small amount of Y_2O_3 having been detected in the powder pattern, this impurity was introduced in the final stages of the refinement. The final refinement, carried out in the range (20–100°2θ), involved the following parameters: five atomic coordinates and five isotropic temperature factors, two scale factors, one zero point parameter, six coefficients were used to describe the functional dependence of the background, three cell parameters (two for $YONO_3$ and one for the cubic Y_2O_3), one asymmetry parameter for each phase, three and two half-width parameters for $YONO_3$ and Y_2O_3 respectively, the line shape factor *m* and two parameters to describe its angular variation for the oxide nitrate phase. The details of the refinement are given in Table 2. Figure 4 shows the final fitting between the observed and calculated patterns.

TABLE 3

Position and Thermal Parameters and Their Standard Deviations for $YONO_3$

Atom	*x*	*y*	*z*	B_{iso} (Å^2)
Y	0.25	0.25	0.8845(3)	0.5(1)
Ox	0.25	0.75	0.	2.1(3)
O1	0.25	0.25	0.457(2)	2.2(3)
O2	0.043(3)	0.75	0.732(2)	2.7(3)
N	0.25	0.25	0.340(3)	4.3(6)

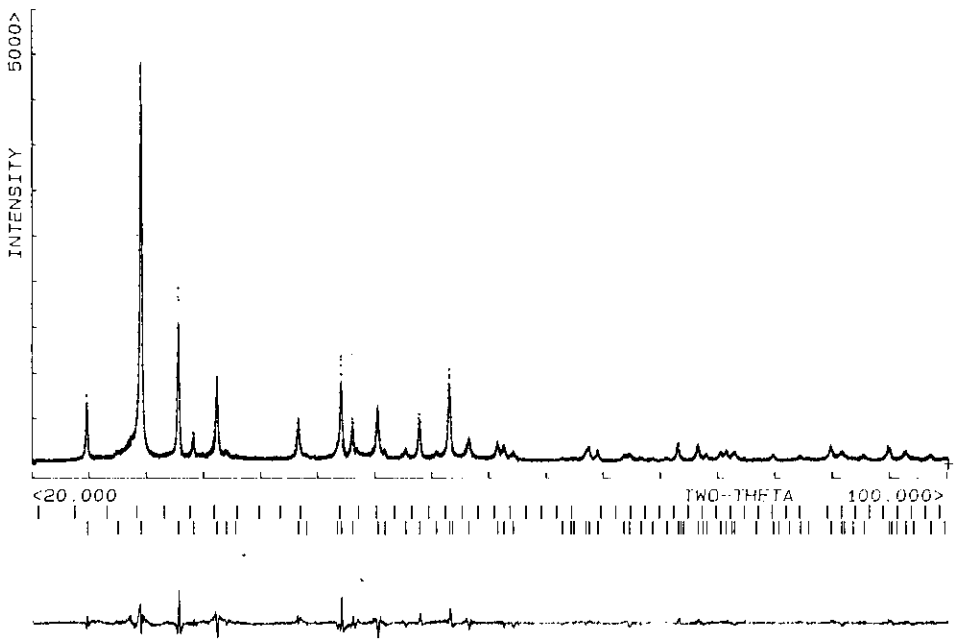

FIG. 4. Final Rietveld difference plot of $YONO_3$. The upper trace shows the observed data as dots and the calculated pattern is shown by solid lines. The lower trace is the plot difference: observed minus calculated. The vertical markers show positions calculated for Bragg reflections (upper part for cubic Y_2O_3, lower part for $YONO_3$).

TABLE 4

Selected Bond Distances (Å) and Angles (°) with Their Standard Deviations for $YONO_3$

Y–O*x* (×4)	2.232 (1)
O2 (×4)	2.56 (1)
N–O1	1.13 (3)
O2 (×2)	1.33 (2)
O1–N–O2 (×2)	122 (1)
O2–N–O2	116 (2)

The discrepancies of greater magnitude observed on the difference curve result clearly from an imperfect modelling of a few lines, a consequence of the anisotropic line broadening reported above. Nevertheless, this fit corresponds to satisfactory crystal structure model indicators (R_F = 0.039, R_B = 0.054) and profile factors (R_p = 0.12, R_{wp} = 0.16). Final atomic coordinates are given in Table 3 and selected distances and angles in Table 4. O*x* corresponds to the isolated oxygen atom and O1, O2 belong to the nitrate group, O2 is the "disordered" atom and has an occupation factor of 0.5.

Description of the Structure and Discussion

The projection of the structure along [100] (Fig. 5) shows the two possible orientations of the nitrate groups owing to the disorder of O2. Let us note that this disorder affects the polyhedra around Y. The possible orthorhombic space group would allow only one orientation, but too short distances (*a*/2 or *b*/2) between two oxygen atoms of two different NO_3 groups (dotted line in Fig. 5) would be obtained. Consequently, the tetragonal *P*4/*nmm* space group is the most convenient because it supposes two alternate orientations of the nitrate groups [parallel to (100) and parallel to (010)], since the Wyckoff site 8*h* is half-occupied by O2. Actually *a* and *b* axes should be doubled to allow the alternation of these two orientations.

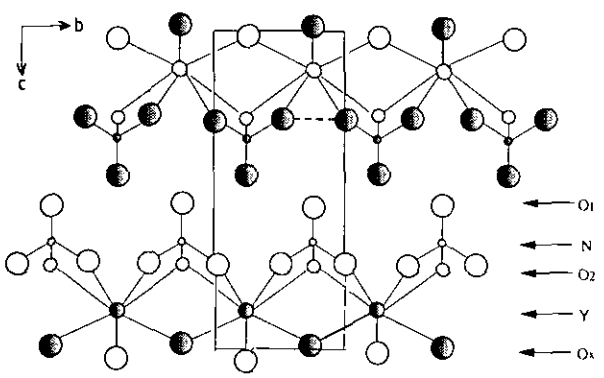

FIG. 5. Projection of the structure along [100]. Shaded circles represent atoms with x = 0.25 and empty circles atoms with x = 0.75, except for some O2 atoms corresponding to the nitrate group perpendicular to the projection plane, for which $x = \pm 0.043$ (smaller circles) and ± 0.467.

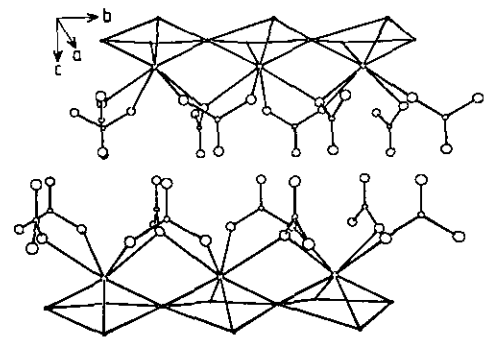

FIG. 6. Perspective view of the structure of $YONO_3$.

Nevertheless, a careful examination of the powder pattern does not show any additional diffraction line corresponding to long range doubling of the *a* and *b* dimensions. So the description of the "average" structure with tetragonal symmetry is certainly the best that can be done. Figure 6 shows a perspective view where the two orientations are alternated. In this case, the shortest O–O contact between two different NO_3 groups has the reasonable value of 2.95 Å.

The structure of $YONO_3$ is closely related to the well known matlockite (PbFCl)-type structure. A number of compounds (among them Y*OX* with *X* = halogen) cristallize with this structure, in which the cation is nine-coordinated. The most electronegative anions form a square pyramid with the cation and the cations constitute a tetrahedron around each anion. This general framework is the same in $YONO_3$ (Fig. 6) where the square planes formed by the O*x* atoms share edges. The N atom lies at the same position that the halogen atom in Y*OX* and the O2 atoms complete to eight the coordination of Y forming a distorted YO_8 square antiprism (in Y*OX* five halogen atoms complete to nine the coordination polyhedra). The Y–O*x* distance (2.23 Å) compares well with 2.29 Å recently reported in $Y_4O(OH)_9NO_3$ (23). The Y–O(NO_3) distance (2.56 Å) is significantly longer. [Note that these distances are ranged from 2.36 to 2.52 Å in the lattices of various yttrium nitrate hydrates (12–14).] The nitrate groups, common to four YO_8 polyhedra, are bridging two Y cations in the [100] and [010] directions as shown in Fig. 5. The terminal atom O1 is not bonded to Y and the N–O1 distance is significantly shorter than the N–O2 distances. Each O2 atom is bonded to two Y atoms.

The $YONO_3$ lattice can be considered as having a layer-type structure, the layers running parallel to (001). The *c*/*a* ratio has been used as criterion for the layer character; its value increases regularly with the size of the halogen in the Y*OX* familly: 1.39 for YOF, 1.69 for YOCl, 2.06 for YOBr, and 2.34 for YOI. The ratio is 2.52 for $YONO_3$.

REFERENCES

1. G. Odent and M.-H. Autrusseau-Duperray, *Rev. Chim. Minér.* **13**, 196 (1976).

2. F. Hulliger. *in* "Structural Chemistry of Layer-Type Phases" (F. Lévy, Ed.) Vol. 5. Reidel, Dordrecht, 1976.
3. D. Louër, J. P. Auffrédic, J. I. Langford, D. Ciosmak, and J. C. Niepce, *J. Appl. Crystallogr.* **16,** 183 (1983).
4. J. I. Langford, A. Boultif, J. P. Auffrédic, and D. Louër, *J. Appl. Crystallogr.* **26,** 22 (1993).
5. D. Louër, R. Vargas and J. P. Auffrédic, *J. Am. Ceram. Soc.* **67,** 136 (1984).
6. A. Boultif, Thesis, University of Rennes, 1993.
7. C. E. Holcombe, *J. Am. Ceram. Soc.* **61,** 481 (1978).
8. Y. M. de Haan, *Nature London* 200 (1963).
9. J. Plévert, J. P. Auffrédic, M. Louër, and D. Louër, *J. Mater. Sci.* **24,** 1913 (1989).
10. D. Louër and J. I. Langford, *J. Appl. Crystallogr.* **21,** 430 (1988).
11. R. Delhez, Th. H. de Keijser, J. I. Langford, D. Louër, E. J. Mittemeijer, and E. J. Sonneveld, *in* "The Rietveld Method," (R. A. Young, Ed), Chap. 8, pp. 132–166. Oxford Univ. Press, London, 1993.
12. B. Eriksson, *Acta Chem. Scand. Ser. A* **36,** 186 (1982).
13. B. Ribar, P. Radivojevic, G. Argay, and A. Kalman, *Acta Crystallogr. Sect. C* **44,** 595 (1988).
14. B. Ribar, P. Radivojevic, G. Argay, and A. Kalman, *Acta Crystallogr. Sect. C* **46,** 525 (1990).
15. J. I. Langford. *in* "Accuracy in Powder Diffraction II, ed. (E. Prince and J. K. Stalick, Eds.) NIST Spec. Publ. No. 846, pp. 110–126. 1992.
16. D. Louër and M. Louër, *J. Appl. Crystallogr.* **5,** 271 (1972).
17. A. Boultif and D. Louër, *J. Appl. Crystallogr.* **24,** 987 (1991).
18. A. D. Mighell, C. R. Hubbard and J. K. Stalick, "NBS*AIDS80: A FORTRAN Program for Crystallographic Data Evaluation," Nat. Bur. Stand. (U.S.) Tech. Note 1141. 1981. [NBS*AIDS83 is an expanded version of NBS*AIDS80]
19. PDF database. ICDD, Newtown Square, PA 1992.
20. J. N. Haschke, *Inorg. Chem.* **13,** 1812 (1974).
21. J. Rodriguez-Carvajal. *In* "Collected Abstracts of Powder Diffraction Meeting," p. 127. Toulouse, France, 1990.
22. D. B. Wiles and R. A. Young, *J. Appl. Crystallogr.* **14,** 149 (1981).
23. A. N. Christensen, M. Nielsen, K. P. J. O'Reilly, and T. Wroblewski, *Acta Chem. Scand.* **46,** 224 (1992).